applied sciences

MDPI

Article

Centrifugal Test Replicated Numerical Model Updating for 3D Strutted Deep Excavation with the Response-Surface Method

Md Mehidi Hassan [1], Jong Seok Yun [1], Md Motiur Rahman [2], Yun Wook Choo [1], Jin-tae Han [3] and Dookie Kim [1,*]

[1] Department of Civil and Environmental Engineering, Kongju National University, Cheonan 31080, Korea
[2] Department of Civil Engineering, Pabna University of Science & Technology, Pabna 6600, Bangladesh
[3] Department of Geotechnical Engineering Research, Korea Institute of Civil Engineering and Building Technology, Goyang-si 10223, Korea
[*] Correspondence: kim2kie@kongju.ac.kr; Tel.: +82-10-9412-9382

Abstract: Centrifugal tests provide an efficacious experimental process to predict the behavior of deep excavations, and numerical models are indispensable for demonstrating the test results and analyzing the engineering demand parameters. Uncertainty in material properties can cause simulations to differ from tests; therefore, updating the model becomes inevitable. This study presents a response-surface-based model updating technique for the nonlinear three-dimensional simulation of the centrifugal testing model of strutted deep excavation in sand. An overview of the fundamentals of the response-surface model is provided, including selecting uncertain parameters as input factors, creating a design order for training the model, building a second-order polynomial surface, and updating the input factors through targeted centrifugal results. The bending strains of diaphragm wall panels at multiple points along the depth are used to form the multiobjective function. Response-surface model predictions were well-matched with actual numerical responses, with less than a 0.5% difference. Parametric analyses could be conducted utilizing this updated strutted deep excavation model.

Keywords: numerical analysis; centrifugal test; response-surface method; strutted excavation; model updating

check for updates

Citation: Hassan, M.M.; Yun, J.S.; Rahman, M.M.; Choo, Y.W.; Han, J.-t.; Kim, D. Centrifugal Test Replicated Numerical Model Updating for 3D Strutted Deep Excavation with the Response-Surface Method. *Appl. Sci.* **2022**, *12*, 10665. https://doi.org/10.3390/app122010665

Academic Editor: Mingguang Li

Received: 29 September 2022
Accepted: 19 October 2022
Published: 21 October 2022

1. Introduction

To preserve the environment, and to maintain a balance between accretive populations and rapid urbanization, the construction of utility skyscrapers and underground structures has recently become a demanding sector. Deep excavation is an essential step for constructing these kinds of facilities. Deep excavation can extend to distances exceeding three kilometers [1]. Strutted or braced excavations are effective methods to ensure enough safety because soil movement and wall deformation characteristics are mainly influenced by unsupported wall span lengths [2]. The displacement and ground settlement characteristics of this complex soil–structure interaction system can only be predicted through empirical and semiempirical methods. So, numerical tools have been introduced to deep strutted excavation analysis. By integrating complex nonlinear soil models, numerical tools were used in deep excavation to investigate the passive soil response [3], strut prestressing effect [4], clay layer depth effect on earth pressure, struts, and walls [5], the lateral effective stress effect during the excavation construction process [6], the consolidation effect [7], the excavation geometry effect against basal heave on three-dimensional ground movements [8], the time-dependent behavior of excavation [9], the penetration depth effect of diaphragm wall [10], and the behavior of braced excavation in the sand [11]. These numerical analyses were performed either on the basis of data from case studies or previous studies. Numerical model development and validation, especially the numerical modeling of centrifugal tests, require highly specialized skills. Very few numerical analyses were performed to predict centrifugal results for the static behavior of deep excavation. Excavation effects on piles [12] and basement excavation effects on an existing tunnel [13] are numerically investigated using centrifugal test data.

Realistic excavation modeling with reliable soil stiffness is still a concerning matter because soil materials usually used in centrifugal modeling differ from field soils [14]. The accuracy of the numerical modeling predominantly depends on the soil character; uncertain soil can generate significant errors in the test results. To minimize error in numerical modeling, the updating of soil parameters with back analysis is usually applied. Back analysis to update the soil parameters for deep excavation is conducted using several approaches, including the Gauss–Newtonian [15], quasi-Newtonian [16], genetic-algorithm [17,18], differential-evolution [19], self-learning simulation [20], probabilistic maximal-likelihood formulation [21] methods, and Bayesian updating [22]. Most of these analyses use a single response and single objective function. Qi and Zhou showed that multiple-point responses can update soil parameters more precisely [23]. Using the Pareto multiobjective optimization technique, Huang et al. updated nine soil parameters in the modified Cam–Clay model [24]. Multiparameter updating using multiple-point responses is a highly complex process, and this analysis is still beyond reach. Back analysis for multiparameter updating using multiple-point responses can be achieved simply through the response-surface method, as there are available software tools for the construction of a response-surface model. The response-surface method has been used as a tool for structural numerical model updating [25] in some aspects, but it has not been used in deep excavation.

In this paper, an approach is established for smooth multiple-parameter updating using multiple-point responses with the response-surface method. Seven bending strain responses along the depth of a wall from the centrifugal test of strutted deep excavation are used for model updating. A framework is proposed to adopt unknown soil parameters in the numerical modeling of centrifugal tests. A numerical model can be established within an optimal amount of time and with optimal cost using this proposed framework.

2. Centrifugal Test

A centrifugal test was carried out for the seismic analysis of strutted excavation at Korea Construction Engineering Development (KOCED) centrifugal facilities. The centrifugal equipment had first been spun to 40 g before seismic loads were input to obtain static analysis data. KOCED had a 5 m radius and 240 g-tons beam centrifugal facilities at the Korea Advanced Institute of Science and Technology (KAIST) [26].

The excavation construction process could be simulated with remote operation through an onboard four-degree-of-freedom flight robot. The KOCED centrifuge at KAIST is shown in Figure 1a. Though the centrifuge had a maximal capacity of 100 g centrifugal acceleration, this experiment was conducted under 40 g. A rectangular equivalent shear beam (ESB) container facilitated the model. The model of strutted excavation is shown in Figure 1b. The installed centrifugal data acquisition system (DAQ) can record strain gauges, voltage, accelerometers, and LVDT readings through 192 channels. Strain gauge data were used for updating the numerical model.

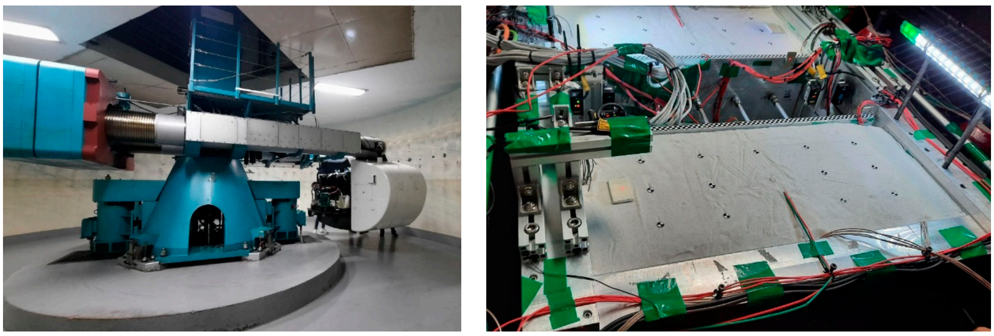

(**a**) (**b**)

Figure 1. Centrifugal test: (**a**) KOCED centrifuge at KAIST; (**b**) centrifugal strutted-excavation model.

2.1. Test Model

A reduced-scale centrifugal model was established where static and dynamic tests were performed to produce the design guideline for the temporary retaining wall. The dimensions of the backfill materials and other structural components are shown in Figure 2. In the centrifugal model, two aluminum alloy (6061) wall panels were used to simulate the diaphragm wall. The geometry of the two wall panels was the same. Each wall panel's width, height, and thickness were 625, 625, and 15.4 mm, respectively. An aluminum alloy plate (6061) with a thickness of 15 mm was rigidly connected to the bottom of the walls, providing a fixed-tip condition.

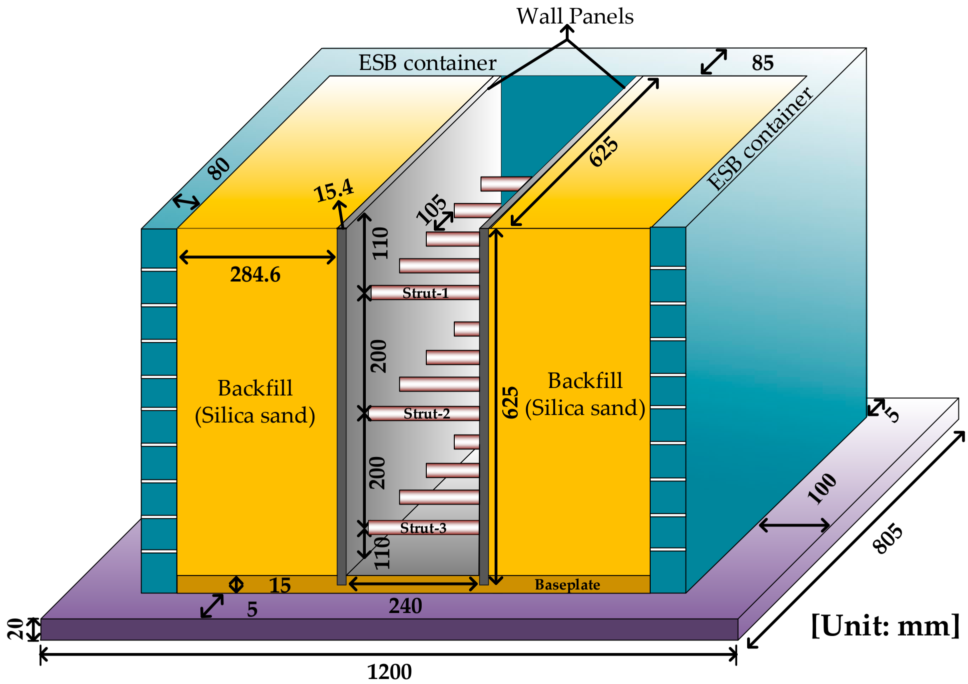

Figure 2. Geometry of strutted excavation.

A total of three-row struts were installed along the depth of the wall. The top strut row was located 110 mm below the top of the wall. Bottom strut rows were located at a 110 mm distance from the bottom aluminum plate. The middle strut row was at an equivalent 200 mm distance from the top and bottom strut rows. Each row had five struts at a 105 mm center-to-center distance. The edge struts of each layer were located at a 102.5 mm distance from the wall edge. A total of 15 aluminum alloy (6061) pipes of 1 mm thickness and 10 mm diameter were used to simulate 15 struts. Each strut length was 240 mm, equivalent to the excavation width. The backfill material was hammer-crushed silica sand. The whole model was placed in an equivalent shear beam (ESB) container.

2.2. Test Result

Bending strain values of the wall panel along the depth were obtained from the strain gauges during the centrifugal test. Figure 3 shows the result from the centrifugal test, where the left graphic shows the location of the strain gauges. The bending strains are presented in the right graphic with the mean values of the filtered data from the centrifugal test. These data were taken when the centrifugal acceleration was equivalent to 40 times Earth's gravity.

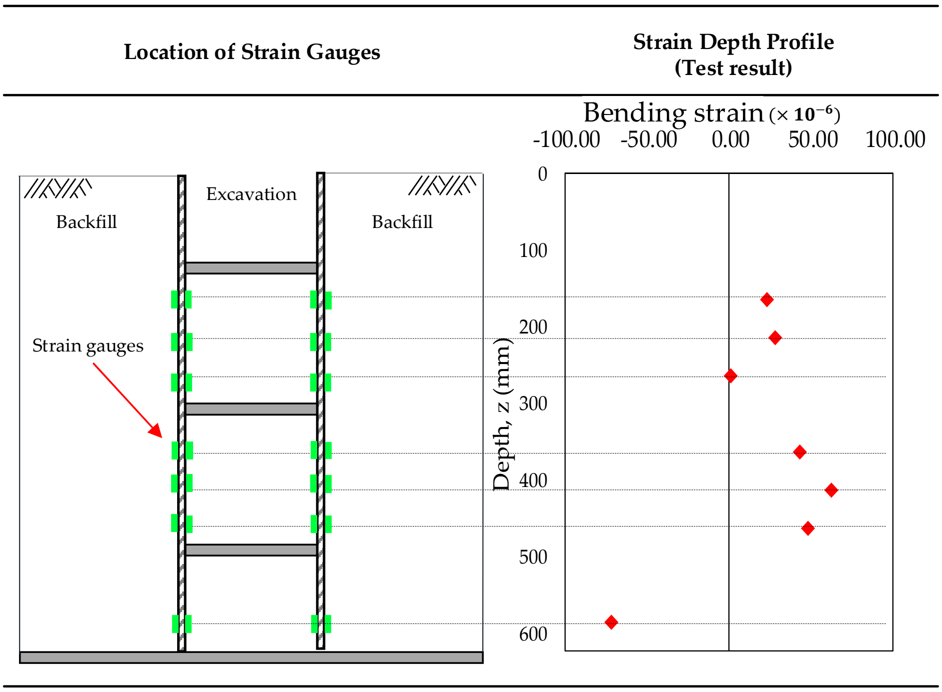

Figure 3. Centrifugal test result.

3. Numerical Model

3.1. Soil and Structure

A 3D numerical model of the centrifugal model was produced using Abaqus software [27]. The physical geometry of the structural elements was similar to that of the centrifugal model. The three-dimensional model mesh is shown in Figure 4, where all the dimensions are presented in millimeter (mm) units. Baseplate, walls, and soil were considered to be 3D solid elements. Beam elements were considered for the struts. The meshes of the baseplate, walls, and soil were solid hexahedral elements (C3D8R), while the struts were line elements (B31).

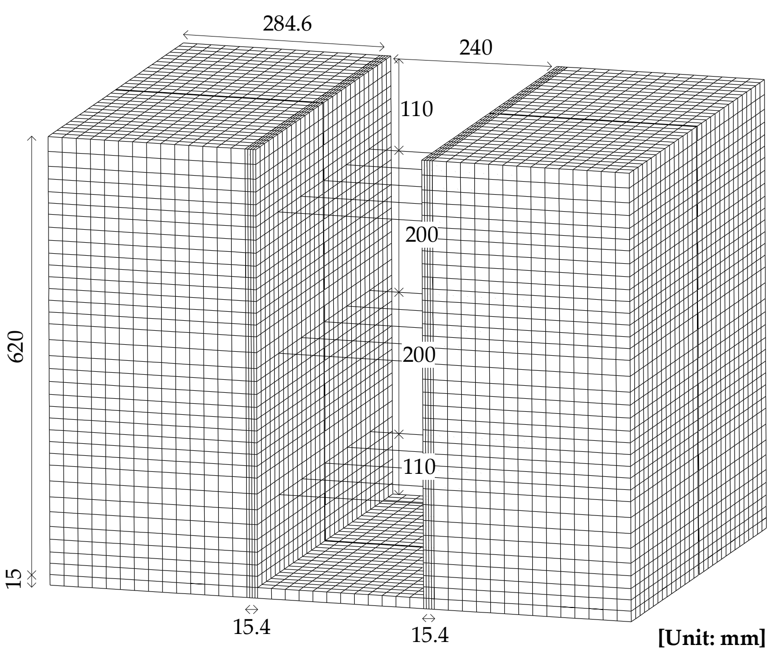

Figure 4. Three-dimensional mesh of the numerical model.

The reduced integration method was used for both types of elements. The mesh had 49,464 nodes and 40,719 elements. Surface-to-surface interaction with finite sliding was established between soil and wall. A similar interaction was also considered for the soil and baseplate. The frictional angle between the soil surface and the wall was regarded as two-thirds of the soil frictional angle. Walls and baseplate were tied where the rotational degree of freedom was also tied. Hinge connections were given between the struts and the wall nodes. The extrapolation of the hinge joints was constrained. As the centrifugal acceleration was equivalent to 40 times Earth's gravity (g) in the centrifugal test, a gravity load equivalent to 40 times that of Earth was adopted vertically. Initial vertical stresses for the backfill materials were adopted in the model. The initial vertical stresses were calculated from $\sigma_{vm} = \rho N g h_m$, where ρ is the soil density, N is the centrifugal acceleration [28], and h_m is the height of the soil.

The lateral displacement of all nodes on the surfaces of the four side's boundaries was constrained in the lateral direction along the normal axis to replace the ESB container as a boundary. Nodes on the bottom surface of the baseplate were constrained in the lateral and vertical directions. Usually, in the 1 g test of a soil sample, the displacement of the box is kept constant for a particular depth to keep the strain similarity between the model and the prototype [29]. However, this test was performed in 40 g condition, so displacement was restricted along the entire depth. The geostatic and static steps were combined for the static analysis of the model.

3.2. Materials

Aluminum alloy (6061) material is perfectly elastic. The available aluminum alloy (6061) with a modulus of elasticity of 68.9 GPa and mass density of 2.7 gm/cm^3 [30] was considered for its properties. The Poisson ratio of the aluminum alloy was assumed to be 0.33. This experiment was conducted using dry silica sand. Mohr–Coulomb plasticity was considered for modeling the nonlinear behavior of silica sand in numerical analysis. A significant range of the parameters of silica sand for the Mohr–Coulomb model was assumed first; then, a response-surface model was created to update these parameters. Very small cohesion yield stress was adopted in the soil model to prevent premature yielding. Absolute plastic strain for sand was considered to be 0. The Poisson ratio of the silica sand is usually considered to be 0.3. The lower and upper ranges of the density of the silica sand were from 1300 to 1800 kg/m^3. The range of the peak frictional angle of the silica sand was from 36.8° to 45.2°, and the critical frictional angle was considered to be 36.6° [31]. The corresponding dilation angle was calculated with Equation (1) [32]:

$$\phi' = \phi'_{crit} + \psi \quad (1)$$

Effective stress affects the nonlinear elasticity of soil, and the modulus of elasticity increases over depth [33]. The elasticity of silica sand is calculated from Janbu's equation [34].

$$E_s = K P_a \left(\frac{\sigma_3{}'}{P_a} \right)^n \quad (2)$$

where $\sigma_3{}'$ denotes the minor effective principal stress, K denotes the stiffness modulus number, P_a is atmospheric pressure, and n is the stiffness modulus exponent. It was reasonable to take the stiffness modulus exponent value as 0.5 [35]. The range of the stiffness modulus number for sand was assumed to be from 100 to 1000. The Earth pressure coefficient in at-rest conditions is calculated from Jacky's equation [36]:

$$K_0 = 1 - sin\phi' \quad (3)$$

Assuming that Poisson's ratio, absolute plastic strain, cohesion yield stress, and the critical frictional angle were comprehensively identical for silica sand, the density, peak frictional angle, and elasticity parameters were updated in this study.

4. Soil Parameter Updating

Soil properties for numerical modeling usually come from the experimental test. Where experimental properties are unavailable, the proposed response-surface-based model updating framework can be an effective solution. The proposed framework is briefly expressed in Figure 5. First, the numerical modeling of the test is conducted. Some properties that usually do not change for particular types of soils were assumed on the basis of previous studies.

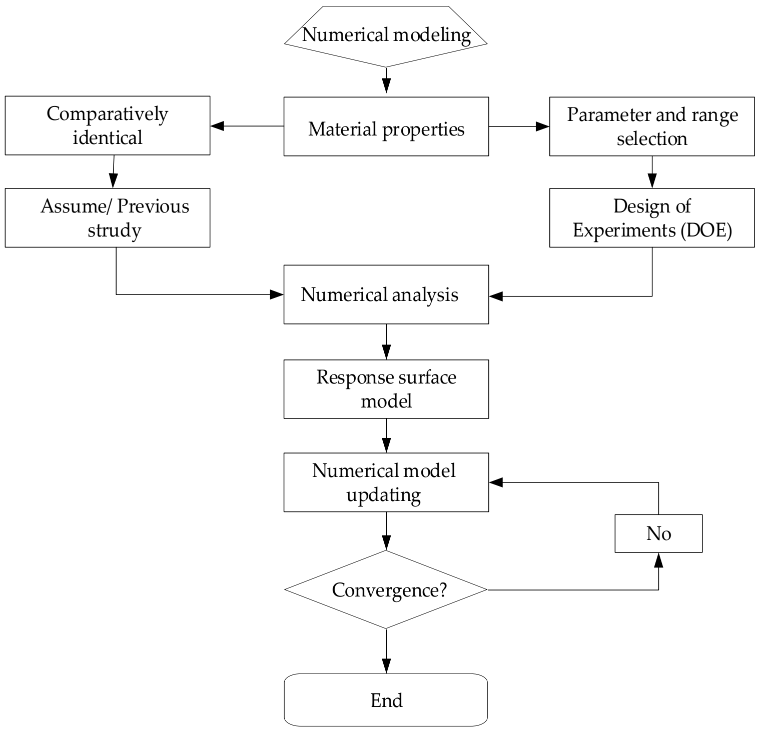

Figure 5. Flowchart of model updating with the response-surface method.

A design order was created for the selected parameters for updating. Numerical analysis was carried out according to the design order. The response-surface model was created by using the design order and corresponding numerical responses. The fitness of the response-surface model was checked with particular criteria. The centrifugal results were set as targets to achieve the corresponding updated soil properties. Lastly, the updated soil properties were adopted in the numerical model.

4.1. Response-Surface Method

The response-surface method (RSM) is an approach with many mathematical processes that dig into the relationship between input factors and output responses. RSM is advantageous not only for cost-efficient and time-saving processes of numerical model updating through optimization [37], but also for the modeling, analysis, and construction of technical models [38]. The relationship between the responses and the independent input variables can be described as follows.

$$S = f(t_1,\ t_2,\ t_3 \ldots\ldots) + z \tag{4}$$

where S is the optimal response that is a function of multiple input variables, t is the input variables, and z is the residual or offsets. The main theme for the response-surface method was developed as a second-order polynomial equation that obtains the optimal response using a series of designed experiments [39]; to solve the curvature system in updating a numerical model, a higher-order polynomial equation should be considered [25]. Second-order polynomial equations are used in this analysis to construct the response surface.

Equation (5) shows the second-order polynomial equation to obtain the optimal response in terms of strain (S).

$$S = u_0 + \sum_{m=1}^{p} u_m t_m + \sum_{m=1}^{p} u_{mm} t_m^2 + \sum_{m=1}^{p} \sum_{m<n}^{p} u_{mn} t_m t_n + z \quad (5)$$

where P is the number of input variables, u_0 is the constant coefficient, u_m is the first-order coefficient, u_{mm} is the pure second-order coefficient, u_{mn} is the intersectional second-order coefficient, and t_m and t_n are the values of input variables. To update multiple variables, the central composite design (CCD) determines how many experiments are conducted [40]. The number of runs for the experiment is determined with Equation (6).

$$N = 2^p + 2p + n_c \quad (6)$$

where 2^p is the cubical points number, $2p$ is the axial points number, n_c is the number of central points, and p represents the number of input variables. The gap between an axial point and the center point is alpha (α). For the p number of input variables in the fully circumscribed central composite design method, α is calculated with Equation (7) [41].

$$\alpha = [2^p]^{1/4} \quad (7)$$

The three-factor orientation of axial and cubical points in a fully circumscribed central composite design is shown in Figure 6. CCD provides six axial points, eight cubical points, and two central points for three input factors.

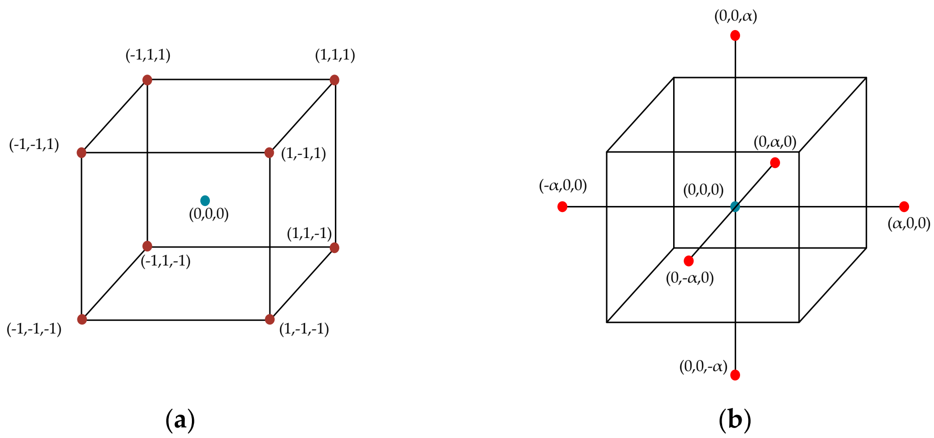

Figure 6. Central Composite Design: (**a**) Cubical point; (**b**) axial point.

4.2. Response-Surface Model

A response-surface model was produced utilizing the Minitab software tool [42] for three input variables, and seven (S1–S7) responses were considered to be targets. Soil density (γ), the frictional angle of the soil (ϕ′), and the stiffness modulus number (K) were considered to be factors or input variables. Ranges of the factors for the cubic, axial, and center points are presented in Table 1.

Table 1. Ranges of the sample values of the input variables.

Factor	Range	Cubic		Axial		Central
		Min.	Max.	Min.	Max.	
γ	Coded	−1	+1	−α	+α	0
	Actual	1396.9	1703.1	1300	1800	1550
ϕ′	Coded	−1	+1	−α	+α	0
	Actual	38.428	43.572	36.6	45.2	40.9
K	Coded	−1	+1	−α	+α	0
	Actual	274.43	825.57	100	1000	550

Fully circumscribed CCD provides 16 design orders for γ, ϕ′, and K, considering two central points and five levels of studies for each factor. The design orders and corresponding responses are shown in Table 2.

Table 2. Design of experiments and corresponding numerical responses.

Run Order	Input Factors			Numerical Responses (Bending Strain $\times 10^{-6}$)						
	γ	ϕ′	K	S1	S2	S3	S4	S5	S6	S7
1	1550.00	45.20	550.00	19.91	23.56	−0.36	31.33	66.31	51.50	−77.01
2	1550.00	36.80	550.00	18.45	22.36	−0.33	29.55	63.03	49.50	−74.32
3	1550.00	41.00	100.00	27.69	30.08	−1.24	43.91	89.28	66.26	−91.90
4	1800.00	41.00	550.00	20.44	23.13	−2.05	31.60	67.98	52.18	−86.90
5	1550.00	41.00	550.00	19.16	22.94	−0.35	30.40	64.59	50.44	−75.64
6	1300.00	41.00	550.00	13.70	20.14	0.76	30.24	62.18	49.44	−64.25
7	1550.00	41.00	1000.00	14.35	18.46	−0.05	22.32	49.55	40.49	−64.46
8	1396.91	38.43	274.43	19.35	24.49	0.04	36.96	75.13	57.74	−76.20
9	1703.09	43.57	274.43	25.54	27.81	−1.89	39.09	81.50	60.85	−93.46
10	1703.09	38.43	274.43	24.29	26.90	−1.92	38.49	80.23	60.15	−92.27
11	1396.91	43.57	274.43	19.82	24.91	0.03	37.75	76.54	58.63	−77.08
12	1703.09	38.43	825.57	17.10	20.41	−0.78	24.63	54.73	43.80	−73.16
13	1396.91	38.43	825.57	13.23	18.44	0.49	24.38	52.40	42.67	−61.51
14	1550.00	41.00	550.00	19.16	22.94	−0.35	30.40	64.59	50.44	−75.64
15	1396.91	43.57	825.57	13.91	19.16	0.51	25.67	54.74	44.20	−63.21
16	1703.09	43.57	825.57	18.22	21.26	−0.89	25.78	56.97	45.10	−75.54

The bending strain as a response to the corresponding factors was adopted in the response-surface model. The relationship between the responses (S1–S7) and factors (γ, ϕ′, K) was developed from Equation (5) as below:

$$S = u_0 + \sum_{m=1}^{3} u_m t_m + \sum_{m=1}^{3} u_{mm} t_m^2 + \sum_{m=1}^{3} \sum_{m<n}^{3} u_{mn} t_m t_n + z \quad (8)$$

So, the second-order polynomial equation became Equation (9).

$$S = u_0 + u_1\gamma + u_2\phi' + u_3K + u_{11}\gamma^2 + u_{22}\phi'^2 + u_{33}K^2 + u_{12}\gamma * \phi' + u_{13}\gamma * K + u_{23}\phi' * K \quad (9)$$

This equation was integrated for the analysis of the response-surface model. The coefficient of the developed equation is listed in Table 3. For each response (S1–S7), these coefficient values were taken from the response-surface model in Minitab software.

Table 3. Values for coefficients.

Coefficient	Coefficient Values for Each Target Equation						
	S1	S2	S3	S4	S5	S6	S7
u_0	19.182	22.941	−0.3531	30.405	64.609	50.454	−75.643
u_1	3.655	1.744	−1.3645	0.6661	2.949	1.3645	−11.44
u_2	0.724	0.595	−0.0144	0.8238	1.545	0.9437	−1.2922
u_3	−5.920	−5.365	0.6143	−10.66	−19.527	−12.69	13.52
u_{11}	−2.193	−1.324	−0.2795	0.494	0.425	0.325	0.08
u_{22}	−0.083	−0.003	0.0165	0.015	0.017	0.015	−0.007
u_{33}	1.757	1.309	−0.2820	2.691	4.762	2.888	−2.525
u_{12}	0.409	0.207	−0.0293	−0.113	−0.077	−0.145	−0.328
u_{23}	−0.832	−0.412	0.4084	−0.839	−1.837	−0.864	2.823
u_{13}	0.028	−0.076	−0.0404	0.349	0.639	0.411	−0.674

This model is trained by the actual response to obtain the best fit and the targeted response. An efficient process for determining the model fitness is analysis of variance (ANOVA) [43]. The *p*-value in ANOVA is the chance of incorrectly rejecting the null hypothesis. A lower *p*-value increases the significance. If the *p*-value is less than 0.05, then the lack of fit can be taken to be insignificant, and a *p*-value greater than 0.1 renders the lack of fit significant [44]. Table 4 depicts that γ, ϕ', K, and $\gamma * \gamma$ were significant model terms for all seven responses.

Table 4. ANOVA of the response-surface model.

Source	DF	*p*-Value						
		S1	S2	S3	S4	S5	S6	S7
Model	9	0.000	0.000	0.000	0.000	0.000	0.000	0.0000
Linear	3	0.000	0.000	0.000	0.000	0.000	0.000	0.0000
γ	1	0.000	0.000	0.000	0.000	0.000	0.000	0.0000
ϕ'	1	0.038	0.013	0.501	0.000	0.000	0.000	0.0000
K	1	0.000	0.000	0.000	0.000	0.000	0.000	0.0000
Square	3	0.004	0.003	0.000	0.000	0.000	0.000	0.0000
$\gamma * \gamma$	1	0.007	0.009	0.000	0.003	0.136	0.055	0.6440
$\phi' * \phi'$	1	0.886	0.993	0.700	0.885	0.948	0.919	0.9680
K ∗ K	1	0.019	0.009	0.000	0.000	0.000	0.000	0.0000
Intersection	3	0.511	0.662	0.000	0.001	0.002	0.003	0.0000
$\gamma * \phi'$	1	0.505	0.588	0.516	0.322	0.775	0.349	0.1060
$\gamma * K$	1	0.200	0.298	0.000	0.000	0.000	0.001	0.0000
$\phi' * K$	1	0.963	0.840	0.378	0.015	0.048	0.028	0.0080

In ANOVA, the goodness of fit (R^2) should not be less than 95% [45]. Table 5 shows that the goodness of fit (R^2) was greater than 95% for all the responses and closely resembled the adjusted goodness of fit (Adj. R^2). The S-value represents the interval between the fitted values and the data values in the units of the output responses.

Table 5. Response-surface method model summary.

Response (Strain)	S-Value	R^2 (%)	Adjusted R^2 (%)
S1	0.6124	99.15	97.80
S2	0.383038	98.70	99.41
S3	0.0450893	99.89	99.74
S4	0.110612	99.99	99.97
S5	0.273217	99.98	99.94
S6	0.151073	99.98	99.96
S7	0.182903	99.99	99.97

Residual plots also examine the fitness of the model. Figure 7 depicts the residual plots for all seven responses. It expresses the outline of the response data in the design order. Normal probability plots provide an expression of the normal distribution of the residuals. Supposing that the normal probability plot forms a straight line, the model could be termed to be adequate [46]. The normal probability plots for all seven responses formed straight lines, so the model was adequate. The residual versus fit plot expresses how the model achieves its target. Each response was uncorrelated from the other, and the observation order indicates that.

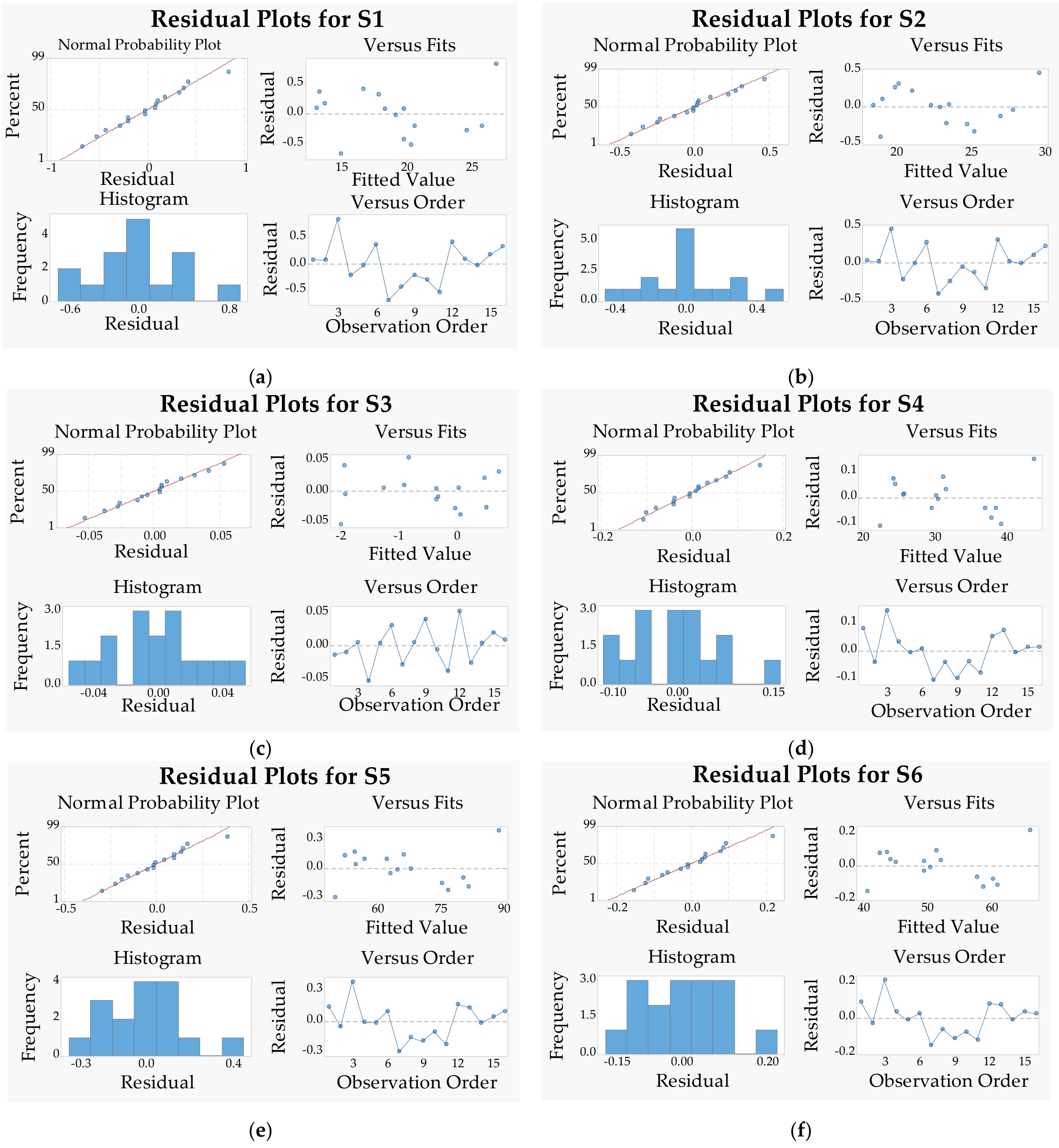

Figure 7. *Cont.*

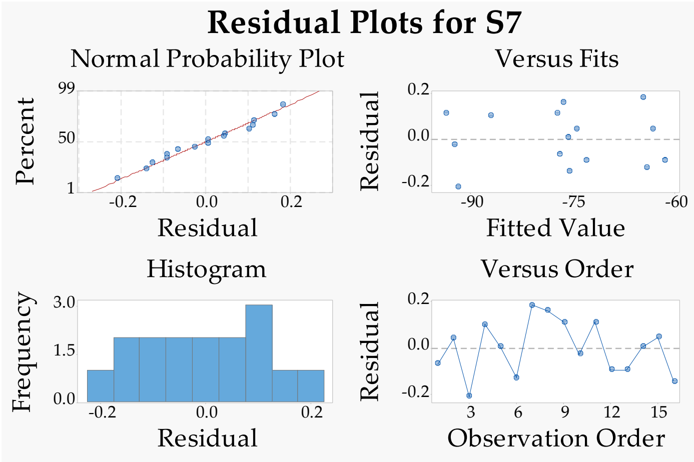

(**g**)

Figure 7. Residual plots: (**a**) S1 response; (**b**) S2 response; (**c**) S3 responses; (**d**) S4 response; (**e**) S5 response; (**f**) S6 response; (**g**) S7 response.

4.3. Updated Properties

For achieving the updated values of γ, ϕ', and K, the responses (S1~S7) target values were assigned in the model. The centrifugal test values were set to be the target values for the responses. The response-surface model provides the updated values of the input factors. Figure 8 shows the updated values for the targeted response. The current level in the figure indicates the best states of the soil properties for which minimal differences with the centrifugal test were achieved. High and low indicate the ranges of the input parameters. The target values was the bending strain results from the centrifugal test. The term y indicates the predicted bending strain responses from the response-surface model for the updated soil properties.

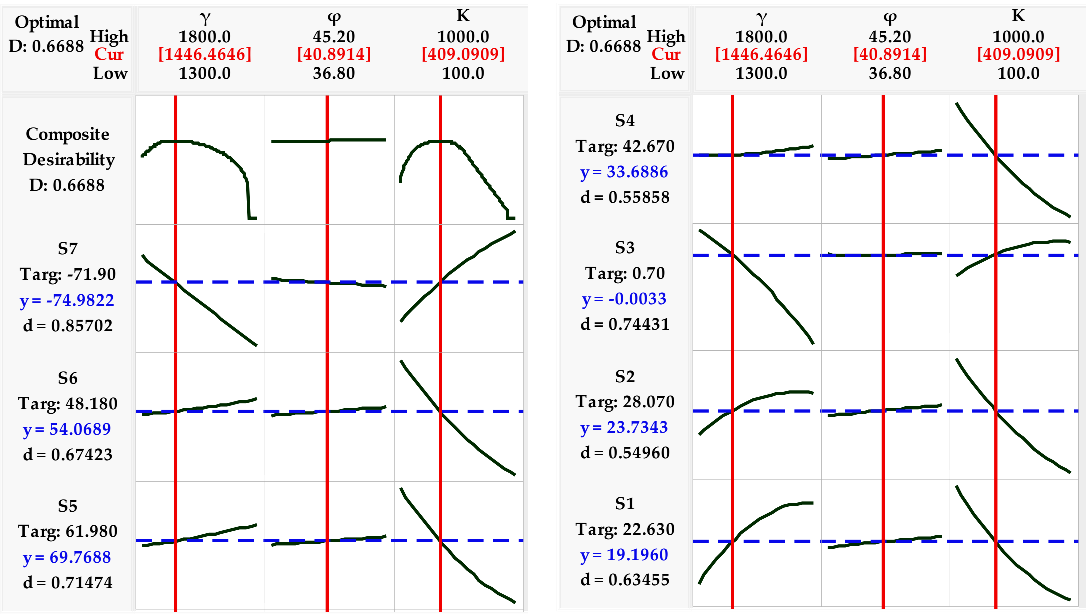

(**a**) (**b**)

Figure 8. Updated properties: (**a**) Responses S4~S7 desirability (**b**) Responses S1~S4 desirability.

The updated values of γ, ϕ', and K from the response-surface model were 1446.46 kg/m^3, 36.67°, and 409.09, respectively. The updated soil parameters were compared with those of previous studies to check whether they were significant for silica sand or not. The soil density and frictional angle values were very close to the results of one of previous tests [47]. The obtained stiffness modulus number value is quite reasonable for fine sand according to Janbu's plots [48]. A comparison is shown in Table 6.

Table 6. Comparison of updated soil parameters with the previous study.

Parameter	Updated	Previous Study	Remark
Density (Kg/m^3)	1446.46	1450	Jo et al. [47]
Frictional angle (°)	40.89	41	Jo et al. [47]
Stiffness modulus number	409.09	350–450	Hoffman [48] (fine sand)

5. Numerical Model Update and Validation

Bending strain and corresponding bending moments are the key parameters for the design of any structure. The bending strain response for particular elements is easier to obtain from a centrifugal test. The numerical model is updated with the bending strain of the wall from the centrifugal test along the depth. The updated soil parameters from the response-surface model are adopted in the numerical model for updating. Figure 9 shows the updated numerical model results. The bending strain of the wall became negative where struts were connected with the wall. The walls were tied with the baseplates that provided fixed tip conditions, so the negative bending strain occurred at the bottom of the wall. The soil in the top layers had the lowest elasticity, and minimal strain occurred in the topsoil layer. However, wall bending strain values at seven particular points were obtained from this updated numerical model for comparison with the centrifugal test.

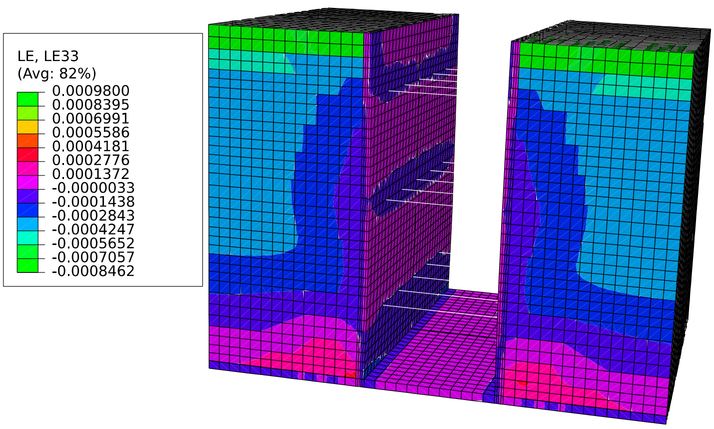

Figure 9. Response (bending strain) of the updated numerical model.

A comparison of the magnitude of the bending strain from the updated numerical model and centrifugal test data is shown in Figure 10. The strain gauges were set at a total of seven locations in the centrifuge; corresponding point responses were taken from the numerical model. In the first segment, the location of those particular points is shown. In the third segment, the differences in the magnitude for the seven points in the centrifuge and numerical model are shown. This showed a good agreement among them with an overall 5.57 ($\times 10^{-6}$) difference in magnitude.

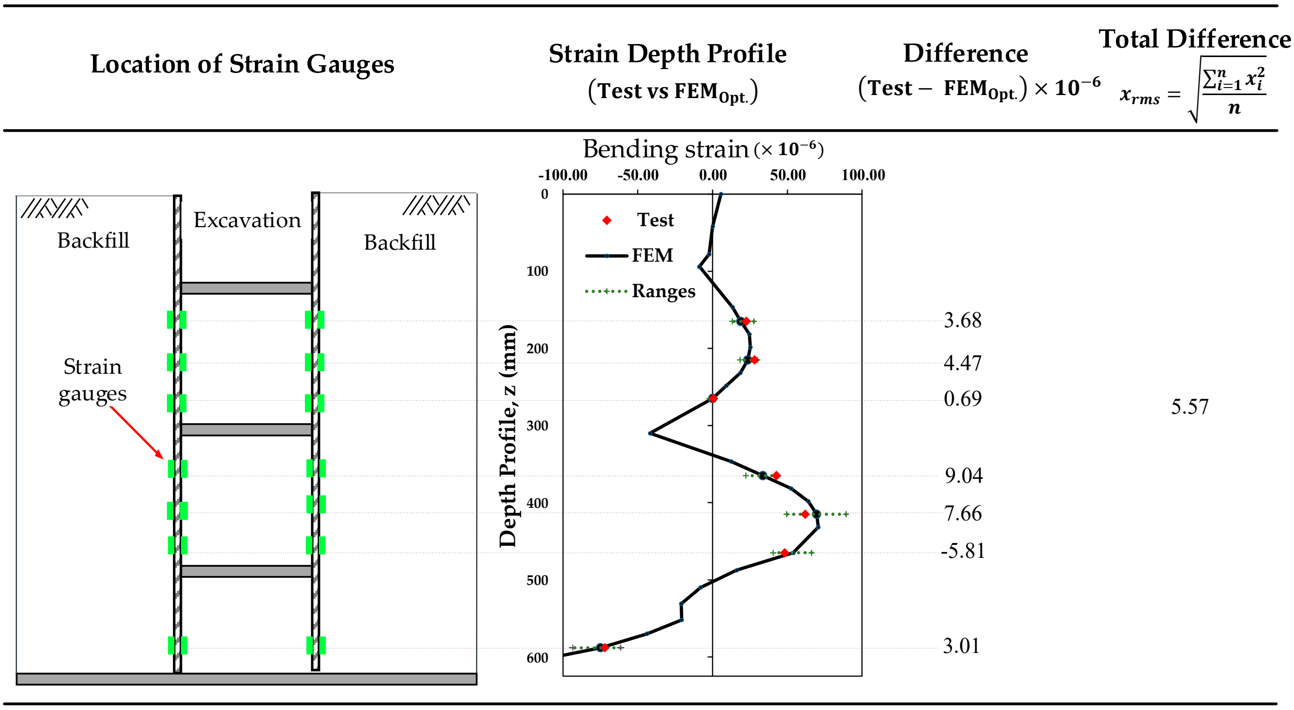

Figure 10. Updated numerical model and test result comparison.

The predicted responses were checked through the corresponding actual responses from the numerical model. Figure 11 shows the linear relationship among them. The response-surface model predictions were quite close to the actual numerical responses, with a difference of less than 0.5%.

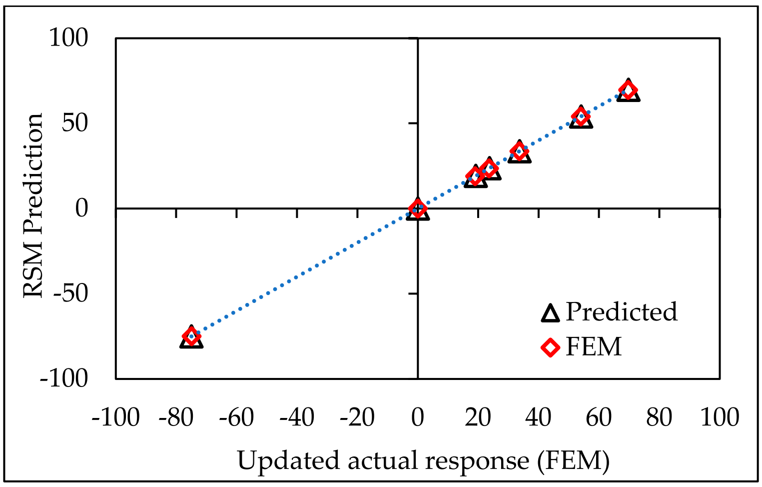

Figure 11. Predicted value vs. updated actual numerical response (FEM) plot.

6. Conclusions

An updated framework of response-surface-based multiobjective model updating for the numerical model of strutted deep excavation in the sand was presented. This proposed framework allows for the adoption of unknown soil parameters in numerical analysis. The process is briefly summarized as follows.

- Comparatively identical properties for particular types of soil were assumed. Suitable ranges for key parameters were selected. The design of experiments (DOE) was created. The structural responses were chosen. Numerical responses were obtained for each DOE. The response-surface (RS) model was created using those responses and

DOE. Centrifugal responses were adopted in the RS model as a target, and updated soil parameters were obtained. The numerical model was updated by adopting the obtained parameters.

- The fitness and significance of the RS model were checked with the coefficient of determination (R^2) and probability values for the obtained results (*p*-value).

A small-scale centrifugal model of strutted deep excavation was numerically designed and updated to investigate this framework. The multiple bending strain values from the strain gauges of the centrifugal test were used as multiple objects to update the soil's three key parameters (density, elasticity, and internal friction). Updated parameters were significant compared to those in previous studies. The key findings of this investigation are summarized below.

- Predictions from the RS model showed good consistency with the numerical model responses; the difference between these two was less than 0.5%.
- The bending strain response of the small-scale numerical model and DOE of the central composite design could establish a well-fitted RS model. This analysis achieved the coefficient of determination (R^2) by more than 95%.
- Minimal differences between the test results and the numerical model were achieved.
- The ranges of the responses could be visualized for the particular ranges of soil properties.
- The updated numerical model showed reasonable agreement with the centrifugal test and it can be used for parametric analysis.

Author Contributions: Conceptualization, M.M.H. and D.K.; data curation, M.M.H. and J.S.Y.; formal analysis, J.S.Y.; funding acquisition, Y.W.C., J.-t.H. and D.K.; investigation, M.M.R.; project administration, Y.W.C., J.-t.H. and D.K.; resources, J.S.Y., J.-t.H. and D.K.; software, M.M.H. and M.M.R.; supervision, Y.W.C. and D.K.; validation, M.M.H.; writing—original draft, M.M.H.; writing—review and editing, M.M.H. and D.K. All authors have read and agreed to the published version of the manuscript.

Funding: This research received no external funding.

Institutional Review Board Statement: Not applicable.

Informed Consent Statement: Not applicable.

Data Availability Statement: Upon request, the corresponding author can supply the data presented in this study.

Acknowledgments: This research was supported by UNDERGROUND CITY OF THE FUTURE program funded by the Ministry of Science and ICT.

Conflicts of Interest: The authors declare no conflict of interest.

References

1. Meng, F.-Y.; Chen, R.-P.; Wu, H.-N.; Xie, S.-W.; Liu, Y. Observed behaviors of a long and deep excavation and collinear underlying tunnels in Shenzhen granite residual soil. *Tunn. Undergr. Space Technol.* **2020**, *103*, 103504. [CrossRef]
2. Yoo, C.; Lee, D. Deep excavation-induced ground surface movement characteristics—A numerical investigation. *Comput. Geotech.* **2008**, *35*, 231–252. [CrossRef]
3. Ou, C.-Y.; Chiou, D.-C.; Wu, T.-S. Three-Dimensional Finite Element Analysis of Deep Excavations. *J. Geotech. Eng.* **1996**, *122*, 337–345. [CrossRef]
4. Bose, S.K.; Som, N.N. Parametric study of a braced cut by finite element method. *Comput. Geotech.* **1998**, *22*, 91–107. [CrossRef]
5. Karlsrud, K.; Andresen, L. Loads on Braced Excavations in Soft Clay. *Int. J. Geomech.* **2005**, *5*, 107–113. [CrossRef]
6. Schäfer, R.; Triantafyllidis, T. The influence of the construction process on the deformation behaviour of diaphragm walls in soft clayey ground. *Int. J. Numer. Anal. Methods Geomech.* **2006**, *30*, 563–576. [CrossRef]
7. Costa, P.A.; Borges, J.L.; Fernandes, M.M. Analysis of A Braced Excavation In Soft Soils Considering The Consolidation Effect. *Geotech. Geol. Eng.* **2007**, *25*, 617–629. [CrossRef]
8. Finno, R.J.; Blackburn, J.T.; Roboski, J.F. Three-Dimensional Effects for Supported Excavations in Clay. *J. Geotech. Geoenvironmental Eng.* **2007**, *133*, 30–36. [CrossRef]

9. Harahap, S.E.; Ou, C.-Y. Finite element analysis of time-dependent behavior in deep excavations. *Comput. Geotech.* **2020**, *119*, 103300. [CrossRef]
10. Bahrami, M.; Khodakarami, M.I.; Haddad, A. 3D numerical investigation of the effect of wall penetration depth on excavations behavior in sand. *Comput. Geotech.* **2018**, *98*, 82–92. [CrossRef]
11. Sankar, S.; Deb, C.K.; Sengupta, A. Estimation of Design Parameters for Braced Excavation: Numerical Study. *Int. J. Geomech.* **2013**, *13*, 234–247.
12. ASHOUR, S.; Ünsever, Y.S. STATIC ANALYSES OF THE EFFECT OF DEEP EXCAVATION ON THE BEHAVIOUR OF AN ADJACENT PILE IN SAND. *Uludağ Üniversitesi Mühendislik Fakültesi Derg.* **2022**, *27*, 627–646. [CrossRef]
13. Ng, C.W.W.; Shi, J.; Hong, Y. Three-dimensional centrifuge modelling of basement excavation effects on an existing tunnel in dry sand. *Can. Geotech. J.* **2013**, *50*, 874–888. [CrossRef]
14. Meng, F.-y.; Chen, R.-p.; Xu, Y.; Wu, K.; Wu, H.-n.; Liu, Y. Contributions to responses of existing tunnel subjected to nearby excavation: A review. *Tunn. Undergr. Space Technol.* **2022**, *119*, 104195. [CrossRef]
15. Finno, R.J.; Calvello, M. Supported Excavations: Observational Method and Inverse Modeling. *J. Geotech. Geoenvironmental Eng.* **2005**, *131*, 826–836. [CrossRef]
16. Tang, Y.-G.; Kung, G.T.-C. Application of nonlinear optimization technique to back analyses of deep excavation. *Comput. Geotech.* **2009**, *36*, 276–290. [CrossRef]
17. Rechea, C.; Levasseur, S.; Finno, R. Inverse analysis techniques for parameter identification in simulation of excavation support systems. *Comput. Geotech.* **2008**, *35*, 331–345. [CrossRef]
18. Levasseur, S.; Malécot, Y.; Boulon, M.; Flavigny, E. Soil parameter identification using a genetic algorithm. *Int. J. Numer. Anal. Meth. Geomech* **2008**, *32*, 189–213. [CrossRef]
19. Zhao, B.; Zhang, L.; Jeng, D.; Wang, J.; Chen, J. Inverse analysis of deep excavation using differential evolution algorithm. *Int. J. Numer. Anal. Methods Geomech.* **2015**, *39*, 115–134. [CrossRef]
20. Hashash, Y.M.A.; Levasseur, S.; Osouli, A.; Finno, R.; Malecot, Y. Comparison of two inverse analysis techniques for learning deep excavation response. *Comput. Geotech.* **2010**, *37*, 323–333. [CrossRef]
21. Wang, L.; Luo, Z.; Xiao, J.; Juang, C.H. Probabilistic Inverse Analysis of Excavation-Induced Wall and Ground Responses for Assessing Damage Potential of Adjacent Buildings. *Geotech. Geol. Eng.* **2014**, *32*, 273–285. [CrossRef]
22. Juang, C.H.; Luo, Z.; Atamturktur, S.; Huang, H. Bayesian updating of soil parameters for braced excavations using field observations. *J. Geotech. Geoenvironmental Eng.* **2013**, *139*, 395–406. [CrossRef]
23. Qi, X.-H.; Zhou, W.-H. An efficient probabilistic back-analysis method for braced excavations using wall deflection data at multiple points. *Comput. Geotech.* **2017**, *85*, 186–198. [CrossRef]
24. Huang, Z.H.; Zhang, L.L.; Cheng, S.Y.; Zhang, J.; Xia, X.H. Back-Analysis and Parameter Identification for Deep Excavation Based on Pareto Multiobjective Optimization. *J. Aerosp. Eng.* **2015**, *28*, A4014007. [CrossRef]
25. Ren, W.-X.; Chen, H.-B. Finite element model updating in structural dynamics by using the response surface method. *Eng. Struct.* **2010**, *32*, 2455–2465. [CrossRef]
26. Kim, D.-S.; Kim, N.-R.; Choo, Y.W.; Cho, G.-C. A newly developed state-of-the-art geotechnical centrifuge in Korea. *KSCE J. Civ. Eng.* **2013**, *17*, 77–84. [CrossRef]
27. Abaqus. *Documentation, 2017*; Dassault Systémes Simulia Corp.: Providence, RI, USA, 2017.
28. Kim, D.-S.; Kim, N.-R.; Choo, Y.-W. Physical modeling of geotechnical systems using centrifuge. In Proceedings of the Korean Geotechical Society Conference, Incheon, Korea, 25–26 September 2009; Korean Geotechnical Society: Seoul, Korea, 2009.
29. Grasso, S.; Lentini, V.; Sammito, M.S.V. A New Biaxial Laminar Shear Box for 1g Shaking Table Tests on Liquefiable Soils. In Proceedings of the 4th International Conference on Performance Based Design in Earthquake Geotechnical Engineering, Beijing, China, 15–17 July 2022; Springer International Publishing: Cham, Switzerland, 2022.
30. Maurya, N.K.; Maurya, M.; Srivastava, A.K.; Dwivedi, S.P.; Kumar, A.; Chauhan, S. Investigation of mechanical properties of Al 6061/SiC composite prepared through stir casting technique. *Mater. Today-Proc.* **2020**, *25*, 755–758. [CrossRef]
31. Kim, J.H.; Choo, Y.W.; Kim, D.J.; Kim, D.S. Miniature Cone Tip Resistance on Sand in a Centrifuge. *J. Geotech. Geoenvironmental Eng.* **2016**, *142*, 04015090. [CrossRef]
32. Bolton, M.D. The strength and dilatancy of sands. *Geotechnique* **1986**, *36*, 65–78. [CrossRef]
33. Khoiri, M.; Ou, C.-Y. Evaluation of deformation parameter for deep excavation in sand through case histories. *Comput. Geotech.* **2013**, *47*, 57–67. [CrossRef]
34. Janbu, N. Soil compressibility as determined by oedometer and triaxial tests. In Proceedings of the European Conference on Soil Mechanics and Foundation Engineering, Wiesbaden, Germany, 15–18 October 1963; Norwegian Geotechnical Institute: Oslo, Norway, 1963.
35. Duncan, J.M. *Strength, Stress-Strain and Bulk Modulus Parameters for Finite Element Analyses of Stresses and Movements in Soil Masses*; Report No: UCB/GT/80-01; University of California: California, CA, USA, 1980.
36. Jaky, J. The coefficient of earth pressure at rest. *J. Soc. Hung. Archit. Eng.* **1944**, *78*, 355–358.
37. Yousefi, M.; Safikhani, H.; Jabbari, E.; Yousefi, M.; Tahmsbi, V. Numerical modeling and Optimization of Respirational Emergency Drug Delivery Device using Computational Fluid Dynamics and Response Surface Method J International Journal of Engineering. *Int. J. Eng.* **2021**, *34*, 547–555. [CrossRef]

38. Myers, R.H.; Montgomery, D.C.; Anderson-Cook, C.M. *Response Surface Methodology: Process and Product Optimization Using Designed Experiments*; John Wiley & Sons: Hoboken, NJ, USA, 2016; ISBN 1118916034.
39. Box, G.E.P.; Wilson, K.B. On the Experimental Attainment of Optimum Conditions. *Breakthr. Stat.* **1951**, *13*, 1–38. [CrossRef]
40. Hang, Y.; Qu, M.; Ukkusuri, S. Optimizing the design of a solar cooling system using central composite design techniques. *Energy Build.* **2011**, *43*, 988–994. [CrossRef]
41. Rahman, M.M.; Nahar, T.T.; Kim, D.; Park, D.-W. Location Sensitivity of Non-structural Component for Channel-type Auxiliary Building Considering Primary-secondary Structure Interaction. *Int. J. Eng.* **2022**, *35*, 1268–1282. [CrossRef]
42. Alin, A. Minitab. *Wiley Interdiscip. Rev. Comput. Stat.* **2010**, *2*, 723–727. [CrossRef]
43. Sahu, N.K.; Andhare, A.B. Multiobjective optimization for improving machinability of Ti-6Al-4V using RSM and advanced algorithms. *J. Comput. Des. Eng.* **2018**, *6*, 1–12. [CrossRef]
44. Baligidad, S.M.; Chandrasekhar, U.; Elangovan, K.; Shankar, S. RSM Optimization of Parameters influencing Mechanical properties in Selective Inhibition Sintering. *Mater. Today Proc.* **2018**, *5*, 4903–4910. [CrossRef]
45. Joglekar, A.M.; May, A.; Graf, E.; Saguy, I. Product Excellence through Experimental Design. In *Product Excellence through Experimental Design*; Springer Science & Business Media: New York, NY, USA, 1991.
46. Noordin, M.Y.; Venkatesh, V.C.; Sharif, S.; Elting, S.; Abdullah, A. Application of response surface methodology in describing the performance of coated carbide tools when turning AISI 1045 steel. *J. Mater. Process. Technol.* **2004**, *145*, 46–58. [CrossRef]
47. Jo, S.-B.; Ha, J.-G.; Yoo, M.; Choo, Y.W.; Kim, D.-S. Seismic behavior of an inverted T-shape flexible retaining wall via dynamic centrifuge tests. *Bull. Earthq. Eng.* **2014**, *12*, 961–980. [CrossRef]
48. Hoffman, P. Contributions of Janbu and Lade as applied to Reinforced Soil. In Proceedings of the 17th Nordic Geotechnical Meeting, Reykjavik, Iceland, 25–28 May 2016.